Response to noise of a vortex based spin transfer nano-oscillator

Eva Grimaldi,[1,2] Antoine Dussaux,[1,*] Paolo Bortolotti,[1,3] Julie Grollier,[1] Grégoire Pillet,[3] Akio Fukushima,[4] Hitoshi Kubota,[4] Kay Yakushiji,[4] Shinji Yuasa,[4] and Vincent Cros[1,†]

[1]*Unité Mixte de Physique CNRS/Thales and Université Paris-Sud 11, 1 Avenue A. Fresnel, 91767 Palaiseau, France*

[2]*CNES, 1 Avenue Edouard Belin, 31400 Toulouse, France*

[3]*Thales Research and Technology, 1 Avenue A. Fresnel, 91767 Palaiseau, France*

[4]*National Institute of Advanced Industrial Science and Technology (AIST) 1-1-1 Umezono, Tsukuba, Ibaraki 305-8568, Japan*

(Received 22 November 2013; revised manuscript received 3 January 2014; published 7 March 2014)

We investigate experimentally and analytically the impact of thermal noise on the sustained gyrotropic mode of vortex magnetization in spin transfer nano-oscillators and its consequence on the linewidth broadening due to the different nonlinear contributions. Performing time domain measurements, we are able to extract separately the phase noise and the amplitude noise at room temperature for several values of dc current and perpendicular field. For a theoretical description, we extend the general model of nonlinear auto-oscillators to the case of vortex core dynamics and provide analytical expressions of the parameters describing the response to noise of the system. From the analysis of our experimental results, we demonstrate the major role of the amplitude-to-phase noise conversion on the linewidth broadening, and propose several solutions to increase even more the spectral coherence of vortex-based spin transfer nano-oscillators.

DOI: 10.1103/PhysRevB.89.104404 PACS number(s): 75.70.Kw, 72.25.Hg, 75.76.+j, 75.78.−n

I. INTRODUCTION

Since the discovery of spin-transfer-induced dynamics, experimental and analytical studies have led to a much better understanding of the microscopic mechanism of the transfer of angular momentum in nanostructures and the magnetization dynamics that are generated [1,2]. One of the objectives is to improve the characteristic of the rf emitted power associated with the magnetization dynamics, that could result in the development of a new type of integrated and tunable frequency source, the so-called spin transfer nano-oscillator (STNO). Such oscillators are based on the conversion of magnetization dynamics into voltage oscillations. Being nanoscale and with an rf frequency from few tens of MHz to few tens of GHz makes them good candidates for telecommunication applications [3,4]. In the scope of understanding both the magnetization dynamics and improvements of rf features, several issues have been addressed: how to excite magnetic modes with a spin polarized current [5–7], how to improve the STNO output power and decrease critical current densities [8], and, eventually, how the spectrum purity is affected by thermal fluctuations and nonlinearities [9–11].

The fundamental mode of vortex magnetization [12,13] called the gyrotropic mode has been intensively studied in STNOs. These magnetization oscillations can be reduced to the dynamics of the vortex core [14] which give rise to large amplitude oscillations with frequencies from 100 MHz up to 2 GHz. In general, it exhibits a relatively small linewidth compared to STNOs based on other excited modes, e.g., a uniform precession. However, the understanding of the linewidth broadening is still a challenge [15,16]. The spin-transfer-torque-induced vortex dynamics in STNOs can be described by its amplitude and phase. As the magnetization dynamics are affected by the exchange of energy with the thermal bath, amplitude and phase get blurred resulting in amplitude and phase noise, and a finite linewidth is measured. To understand the origin of this linewidth broadening, in Sec. II we present the experimental results corresponding to the amplitude and phase noise of the gyrotropic motion at room temperature from single-shot time domain measurements [17–19]. In Sec. III, we extend a general model of an auto-oscillator [20–24] for our case of interest that corresponds to the case of vortex magnetization dynamics. One of the important results is that we provide analytical expression of the main parameters that describe the response to noise of the vortex-based oscillator. Finally, in Sec. IV we compare experiments and theoretical predictions allowing us to validate the model in the case of vortex dynamics. From this comparison, we can determine the main source of noise. Consequently we propose some solutions to improve furthermore the spectral coherence of vortex-based STNOs in order to reach the characteristics required for integrated rf nanosources.

II. EXPERIMENTAL MEASUREMENTS OF THE LINEWIDTH: FREQUENCY VS TIME DOMAIN

The studied samples are circular tunnel junctions made of a layered stack //synthetic antiferromagnet (SAF)/MgO (1.075)/NiFe (5) (with thickness in nm) of radius $R = 250$ nm. The NiFe free layer has a vortex distribution magnetization with the vortex core polarity set by the external out-of-plane field direction and the chirality set by the dc current induced Oersted field. The SAF is composed of PtMn (15)/CoFe (2.5)/Ru (0.85)/CoFeB (3), and its top layer magnetization is uniform and lies in the film plane. The vortex core position is converted into a voltage via the tunnel magnetoresistance (TMR=15% at room temperature). When an external magnetic field $H_\perp$ is applied perpendicular to the film plane, the SAF top layer magnetization is tilted out of the plane. This gives the

*Department of Physics, ETH Zurich, Schafmattstrasse 16, 8093 Zurich, Switzerland.

†vincent.cros@thalesgroup.com

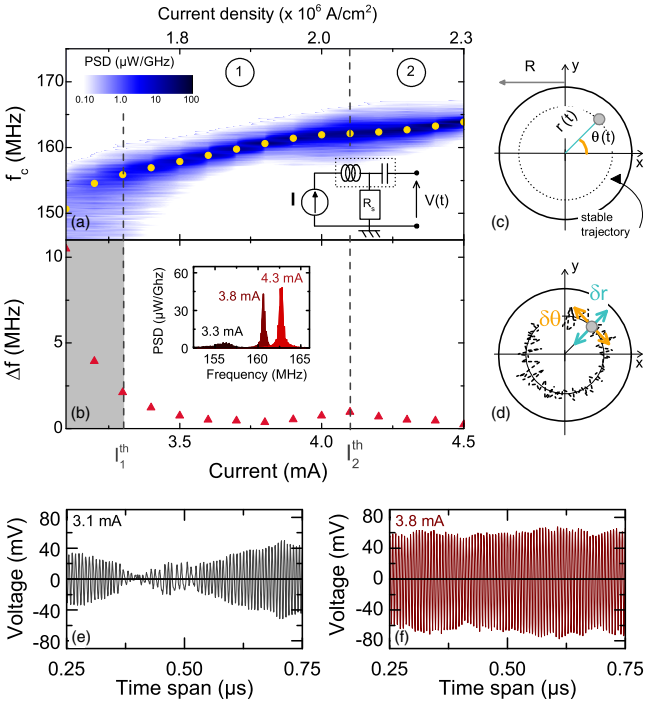

FIG. 1. (Color online) Rf characteristics of a vortex-based STNO measured for $H_\perp = 4.4$ kOe: (a) Color scale of the PSD vs current and (yellow dots) carrier frequency f_c extracted from fit. Inset: Schematic of the measurement set-up. The R_s resistance represents the STNO resistance, and $V(t)$ is the input measurement voltage. (b) Δf vs current. Inset: Voltage PSD measured for 3.3, 3.8 and 4.3 mA. (c) Schematic of the vortex core sustained trajectory described by amplitude $r(t)$ and phase $\theta(t)$. (d) Schematic of vortex core dynamics affected by amplitude noise δr and phase noise $\delta\theta$. (e) An example of time trace below I_1^{th} at 3.1 mA. (f) An example of time trace above I_1^{th} at 3.8 mA. Time traces are measured with a 30 dB amplifier.

necessary spin polarization component of the spin transfer torque to sustain the gyrotropic motion with an uniformly spin polarized current [8,25]. We have performed a comprehensive study at different field values. In this paper, we focus on the data that have been measured at $H_\perp = 4.4$ kOe, but similar conclusions have been obtained for the other field values. Our current convention is that for a positive current, electrons are flowing from the free NiFe layer to the SAF layer. Using a spectrum analyzer, we measure at room temperature the STNO voltage power spectral density plotted in color scale in Fig. 1(a). The measurement setup is shown in the inset in Fig. 1(a).

The vortex core dynamics is described by the evolution in time of its orbit radius $r(t)$ and phase $\theta(t)$ as schematized in Fig. 1(c). Experimentally, we extract the voltage rf properties, i.e. the carrier frequency f_c, the integrated power, and the full width at half maximum Δf, from a Lorentzian fit of the power spectral density of the measured voltage. These quantities are linked to the vortex core dynamics: f_c corresponds to the oscillation frequency of the core $\dot{\theta}/2\pi$, the integrated power is proportional to the normalized orbit radius of the core $s(t) = r(t)/R$, and the linewidth Δf is related to the orbit stability (for details see Appendix A). The stable orbit is perturbed by noise through amplitude noise $\delta s(t) = \delta r(t)/R$ (radial perturbations) and phase noise $\delta\theta$ (orthoradial perturbations along the sustained trajectory) as sketched in Fig. 1(d). The conversion of the vortex dynamic noise into the voltage noise is detailed in Appendix A and it is assumed that the voltage normalized amplitude noise $\delta\alpha$ (resp. the voltage phase noise $\delta\phi$) is equal to the magnetization normalized amplitude noise $\delta s(t)/s_0$ (resp. the magnetization phase noise $\delta\theta$).

In Figs. 1(a) and 1(b), we plot the evolution of the frequency carrier f_c and of the linewidth Δf of the rf signal as a function of the injected current I. Below the current $I_1^{\text{th}} = 3.3$ mA, we measure a large Δf corresponding to large-amplitude vortex oscillations, but these are in fact not continuously sustained over long time scales as plotted in Fig. 1(e). Above I_1^{th} up to $I_2^{\text{th}} = 4.1$ mA, defined as region ① in Figs. 1(a) and 1(b), the vortex core exhibits large-amplitude sustained oscillations induced by spin transfer [see a typical time trace in Fig. 1(f)]. In this region, increasing the current corresponds to a decrease in Δf from 2 MHz down to 360 kHz at $I = 3.8$ mA. For current values close to I_2^{th}, we observe an increase of Δf and a flattening of the frequency carrier evolution: the region ② defined for high currents, above I_2^{th}, corresponds to large-amplitude oscillations (50% of the radius) and large velocity ($\simeq$130 m/s) where a substantial change of the vortex core shape occurs. For this region, our analytical description is no longer valid. The vicinity of I_2^{th} corresponds most probably to a transition region towards another dynamical regime, which implies a change in the linewidth evolution [26]. In the following, we focus on the regime of vortex oscillations corresponding to region ① where a single mode exists. Under the assumption of a single mode excited by spin transfer torque, both the integrated power and carrier frequency evolution have been previously well described analytically [27]. However, there are still some open questions, for example in recent works [16,28,29], it was shown that the linewidth Δf decreases linearly with decreasing temperature down to about 100 K, as expected from fluctuation-dissipation theory, but then it saturates. Thus, the detailed mechanisms at the origin of the linewidth broadening in such vortex-based oscillators, as well as the evolution of the linewidth Δf, remain to be understood.

In the following, we investigate the linewidth Δf broadening under conditions for the applied perpendicular field and dc current for which the sustained oscillations are obtained [region ① in Figs. 1(a) and 1(b)]. The spectral quality of the vortex-based STNO can be investigated quantitatively by separating the voltage amplitude noise $\delta\alpha(t)$ and the voltage phase noise $\delta\phi(t)$ from the voltage output signal $V(t) = V_0[1 + \delta\alpha(t)]\cos[2\pi f_c t + \delta\phi(t)]$ [30]. The phase noise has been previously measured for vortex-based STNOs by Keller *et al.* [31]. However, because of the nonlinear nature of STNOs, the amplitude-phase coupling makes the additional measurement of amplitude noise of significant importance to fully analyze the spectral coherence of vortex-based oscillators.

To perform the analysis of phase and amplitude noise, we measured a 20.5 ms long STNO output voltage time trace with a single-shot oscilloscope over 41×10^6 points at a sampling rate of 2 gigasamples per second. The STNO output voltage $V(t)$ is amplified before the oscilloscope input (gain of 30 dB and noise figure of 1.8 dB). An internal

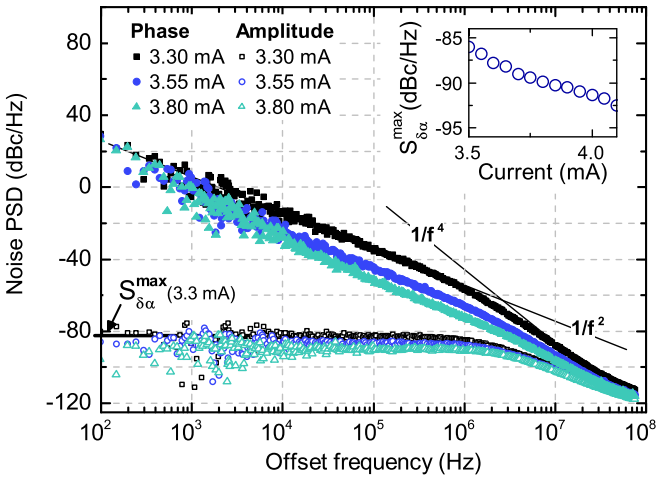

FIG. 2. (Color online) Amplitude (empty dots) and phase (full dots) noise PSD at $H_\perp = 4.4$ kOe obtained for different values of current I (in mA): 3.30 (black squares), 3.55 (blue circles), and 3.80 (green triangles) that correspond respectively to STNO output voltage integrated power of 11, 15, and 23 nW. Inset: Amplitude noise maximum level vs current I.

filter of the oscilloscope is applied to remove frequencies higher than the fundamental gyrotropic mode. By applying the Hilbert transform method that has been recently applied for characterizing the noise in STNO based on uniform magnetization dynamics [17–19], we are able to extract the phase and amplitude noise. In Fig. 2, we plot in logarithmic scale the power spectral density (PSD) of amplitude and phase noise as a function of the offset frequency from the carrier frequency $(f - f_c)$ for 3.30, 3.55, and 3.80 mA. The noise PSDs are limited by the electrical Johnson-Nyquist noise floor increased by the amplifier noise figure around -120 dBc/Hz at offset frequencies above 10^7–10^8 Hz. The amplitude noise is much lower than the phase noise below 1 MHz demonstrating that the phase noise is indeed the main contribution to the linewidth Δf in vortex-based STNOs, as it is the case for most oscillating systems in nature. For all currents, the amplitude noise PSD shows a Lorentzian distribution. At small current I, the phase noise PSD presents a $1/f^2$ dependence at small offset frequencies and a $1/f^n$ (with $2 < n \leqslant 4$) at higher offset frequencies. When the current increases, the amplitude noise maximum level $S_{\delta\alpha}^{\max}$ decreases (see the inset in Fig. 2): the STNO output voltage V_0 increases and the relative amplitude noise, $\delta V/V_0 = \delta\alpha$, decreases. Thus at higher currents, the amplitude noise decreases, and the phase noise PSD tends to a single $1/f^2$ distribution over the whole frequency range which is equivalent to a white frequency noise. This trend of phase noise PSD is a signature of the amplitude-phase coupling due to the nonlinearities and is discussed in the following section.

III. VORTEX MAGNETIZATION DYNAMICS IN THE FRAMEWORK OF THE NONLINEAR AUTO-OSCILLATOR

The amplitude noise and phase noise were analyzed with a general model proposed for nonlinear auto-oscillators [20–24] that takes into account the nonlinear behavior of the system and showed that the linewidth is due to both thermally driven phase noise and amplitude-phase coupling. In this paper, we demonstrate that such an approach is relevant for vortex-based STNOs too.

To understand the linewidth broadening of the STNO and the phase noise distribution, the magnetization oscillations must be considered and studied as nondeterministic dynamics. A general model for nonlinear auto-oscillators [21,23] developed by Slavin and Tiberkevich considered that the deterministic dynamics of a nonlinear oscillator can be described by the equation of the complex amplitude $c(t)$:

$$\frac{dc}{dt} + i2\pi f(p)c + \Gamma_+(p)c - \Gamma_-(p)c = 0, \qquad (1)$$

with f the instantaneous frequency of the oscillator, Γ_+ the positive damping rate that represents the losses of the system, and Γ_- the negative damping rate that represents the gain of the system. These three parameters might depend on the oscillation power $p = |c|^2$. Solving the equation $\Gamma_-(p) = \Gamma_+(p)$ gives the stationary solution for the oscillation power p_0. Moreover, this general model is a powerful tool in the case of nondeterministic dynamics induced by temperature [22,32–34]. The response-to-noise of the system around its stable trajectory can be described with three key parameters: the damping rate for small power deviations from the stationary solution $\pi f_p = [\frac{d\Gamma_+}{dp}(p_0) - \frac{d\Gamma_-}{dp}(p_0)]p_0$, which gives the rate at which the system goes back to the stable trajectory when perturbed; the auto-oscillator generation linewidth in the linear regime $2\Delta f_0 = \frac{1}{2\pi}\frac{k_B T}{\epsilon(p_0)}\Gamma_+(p_0)$ (with $\epsilon(p)$ the energy of the system), which is the intrinsic phase noise due to the thermal energy; and the normalized dimensionless nonlinear frequency shift $\nu = \frac{N}{\pi f_p}p_0$ (with the nonlinear frequency shift coefficient $N = 2\pi\frac{df(p)}{dp}$), which quantifies the coupling between phase and amplitude. Recently, it was demonstrated that this general model could be adapted to STNOs with uniform magnetization dynamics: the predicted results for a white noise affecting the magnetization dynamics described by Eq. (1) were in good agreement with the phase and amplitude noise obtained experimentally [19,29,35].

We have shown recently [27] that for vortex-based STNOs, the spin-transfer-torque-induced gyrotropic motion of the vortex core can be very well described by the Thiele equation [14] considering the higher-order terms of damping and confinement. This allows a deterministic description of the vortex magnetization dynamic frequency and amplitude through the polar coordinates of the vortex core $[s(t),\theta(t)]$ in the normalized disk [see Fig. 1(c)]:

$$\frac{d\theta}{dt} = \frac{\kappa}{G}(1 + \zeta s^2), \qquad (2)$$

$$\frac{ds}{dt} = \frac{D\kappa}{G^2}s\left[\frac{a_j I G}{D\kappa\pi R^2} - 1 + (\zeta + \xi)s^2\right], \qquad (3)$$

with R the radius of the ferromagnetic disk, G the gyrovector magnitude, $D(1 + \xi s^2)$ the damping coefficient with D its linear part and ξ its nonlinearity factor, a_j the spin transfer

torque efficiency, I the current, and $\kappa(1+\zeta s^2)$ the confinement stiffness with κ its linear part and ζ its nonlinearity factor. The confinement stiffness is expressed in terms of the magnetostatic confinement $\kappa_{\rm ms}$, the confinement due to the Zeeman interaction of the in-plane vortex magnetization with the Oersted field $\kappa_{\rm oe} I/\pi R^2$, and the nonlinearity factors $\kappa'_{\rm ms}$ and $\kappa'_{\rm oe} I/\pi R^2$ where $\kappa = \kappa_{\rm ms} + \kappa_{\rm oe} I/\pi R^2$ and $\zeta = \frac{(\kappa'_{\rm ms}+\kappa'_{\rm oe} I/\pi R^2)}{(\kappa_{\rm ms}+\kappa_{\rm oe} I/\pi R^2)}$ (see Appendix B for more details). This description was shown to be in good agreement with the evolution with current and field observed in micromagnetic simulations [27] and with experimental results [36].

Here we derive the general auto-oscillator in Eq. (1) for the particular case of vortex magnetization dynamics in STNOs in the presence of a white noise. The auto-oscillator equation [Eq. (1)] and the equations of phase [Eq. (2)] and amplitude dynamics [Eq. (3)] are equivalent when writing $c(t) = s(t)e^{-i\theta(t)}$, where the vortex oscillation power is $p(t) = s(t)^2$. By identification, we deduce the damping rates specific to the vortex dynamics in a STNO:

$$\begin{aligned}\Gamma_+(p) &= \frac{D\kappa}{G^2}\left[1+(\zeta+\xi)p\right],\\ \Gamma_-(p) &= \frac{a_j I}{G\pi R^2}.\end{aligned} \tag{4}$$

The negative damping rate Γ_- only depends on the injected current I and is independent of the power p. Thus the existence of a stable solution p_0 that verifies $\Gamma_-(p_0) = \Gamma_+(p_0)$ for different currents is allowed due to adjustment of the confinement (proportional to I) and of the nonlinearities (proportional to p_0). The resulting stable solution is a perfect circular trajectory of the vortex core:

$$p_0 = s_0^2 = \frac{\frac{a_j I G}{D\kappa\pi R^2} - 1}{\zeta+\xi}, \tag{5}$$

and has an energy $\epsilon(p_0) = \frac{1}{2}\kappa R^2 p_0$.

An important feature specific to vortex-based STNOs has to be emphasized and compared to uniform magnetization based STNOs. For uniform-based STNOs, the relatively large tunability comes from nonlinearities through the nonlinear frequency shift coefficient N [21]. As a consequence, the linewidth is strongly broadened due to these nonlinearities [11]. In contrast, for vortex-based STNOs, there exist two origins of the frequency tunability which arise from both the confinement term [27,37,38] $\frac{\kappa_{\rm oe} I}{\pi R^2}$ and the nonlinear frequency shift coefficient defined as

$$N = \zeta\frac{\kappa}{G} \tag{6}$$

due to the nonlinearity of the confinement. Thus vortex-based STNOs present a relatively large tunability (10 MHz/mA) with a small nonlinear frequency shift coefficient N, resulting in a narrow linewidth Δf.

To describe the effects of thermal fluctuations on the vortex core dynamics, we express analytically the parameters that govern the response to noise of the nonlinear vortex-based oscillator:

$$\pi f_p = \frac{a_j I}{G\pi R^2} - \frac{D\kappa(I)}{G^2}, \tag{7}$$

$$2\Delta f_0 = \frac{k_B T}{\pi R^2 p_0}\frac{D}{G^2}\left[1+(\zeta+\xi)p_0\right], \tag{8}$$

$$\nu = \frac{\zeta}{\frac{D}{G}(\zeta+\xi)} \tag{9}$$

Finally, similarly to Quinsat *et al.* [19] for the case of uniformly magnetized STNOs, we can express the PSD of phase noise $\delta\theta$ and of normalized amplitude noise $\delta s/s_0$ of the vortex magnetization dynamics:

$$S_{\delta s/s_0} = \frac{\Delta f_0}{2\pi}\frac{1}{f^2+f_p^2} \tag{10}$$

$$S_{\delta\theta} = \frac{\Delta f_0}{\pi f^2} + 2\nu^2\frac{{f_p}^2}{f^2}S_{\delta s/s_0} \tag{11}$$

In summary, the phase noise of the vortex magnetization dynamics in Eq. (11) has two contributions: the intrinsic phase noise that originates directly from a pure thermal phase noise proportional to Δf_0 and the contribution that comes from the conversion of the amplitude noise into phase noise through the coupling factor $(\nu f_p)^2$.

IV. RESULTS AND DISCUSSIONS

In this section we analyze the noise PSD in light of the framework described in the previous section. We present the analysis of the experimental data obtained for several currents. In Fig. 3, the PSDs of amplitude noise and phase noise measured for $I = 3.6$ mA are plotted (see symbols). The black lines are fits to Eqs. (10) and (11): The amplitude noise is fitted with Eq. (10) to extract the parameters f_p and Δf_0. Then, by injecting these parameters into Eq. (11), the phase noise is fitted giving the normalized dimensionless nonlinear frequency shift ν. Note that at a small offset frequency, the phase noise experimental data deviate from the analytical

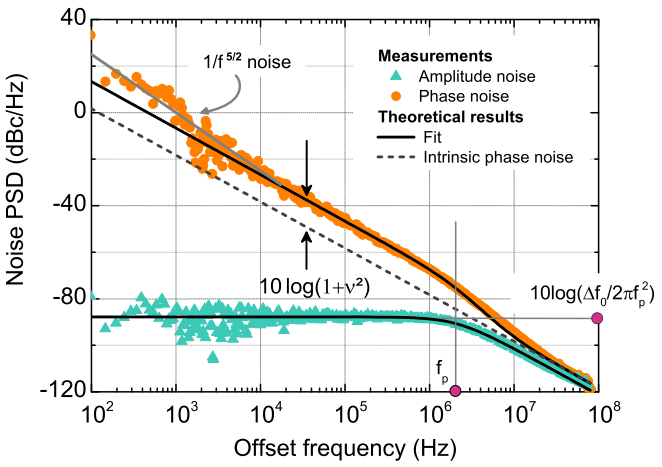

FIG. 3. (Color online) Phase (orange dots) and amplitude (green triangles) noise PSD in dBc/Hz for $I = 3.6$ mA and $H_\perp = 4.4$ kOe. Solid lines correspond to the theoretical amplitude and phase noise PSD from Eqs. (10) and (11) for the response-to-noise parameters $f_p = 2.1$ MHz, $\Delta f_0 = 46$ kHz, and $\nu = 3.7$. The dotted line corresponds to the intrinsic phase noise $\Delta f_0/\pi f^2$. The amplitude-to-phase noise conversion corresponds to an increase of the phase noise of 12 dB.

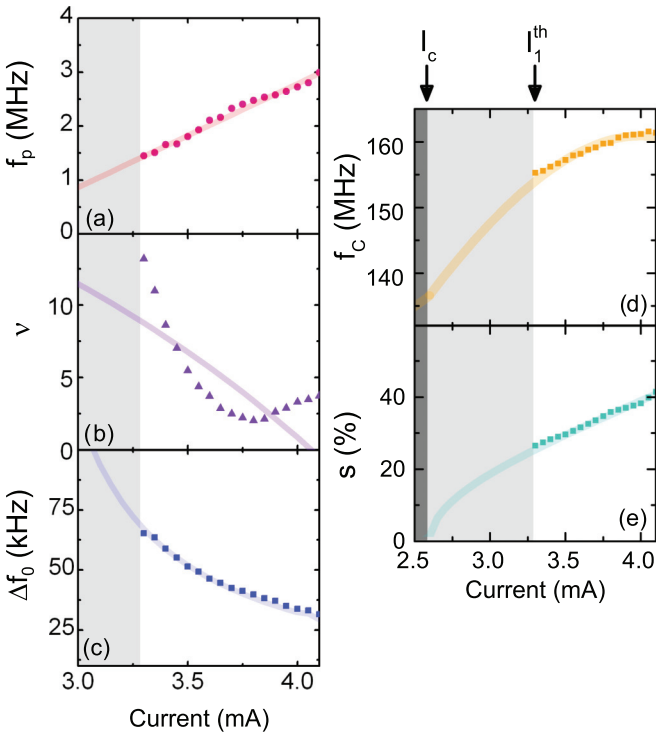

FIG. 4. (Color online) Response-to-noise parameters versus current f_p (a), ν (b) and Δf_0 (c). Vortex dynamic features versus current: carrier frequency (d) and normalized orbit radius (e) for $H_\perp = 4.4$ kOe. The symbols correspond to measurement data, and the solid lines to theoretical curves.

prediction (see gray line of $1/f^{5/2}$ slope). Despite the lack of accuracy at small offset frequencies due to the measurement method, this additional low frequency noise might come from the MgO barrier [39] but is beyond the scope of our analysis, because only noise coming from the magnetization dynamics is considered. Moreover, in region ② in Figs. 1(a) and 1(b), the amplitude and phase noise PSDs correspondingly might be fitted with the Eqs. (10) and (11). However, the parameters that could be extracted from the fitting (not shown here) clearly indicate that the dynamics cannot be described by the gyrotropic motion of a rigid vortex core. Furthermore, in this complex regime, for currents higher than 5.0 mA, an additional $1/f^2$ noise is observed on the phase noise.

In Fig. 4, we plot the response-to-noise parameters f_p, Δf_0, and ν (symbols) extracted for different values of current in region ① with the method presented above. The damping rate for small power deviations πf_p is of the order of 1 MHz and increases linearly with current. The normalized dimensionless nonlinear frequency shift ν decreases sharply down to 2 at 3.8 mA and then increases as it gets close to region ②. The generation linewidth in the linear regime $2\Delta f_0$ is of order 100 kHz and decreases with current down to 64 kHz. The evolution of f_p and Δf_0 with current leads to a decrease of $\frac{\Delta f_0}{2\pi f_p{}^2}$, which corresponds to the amplitude noise PSD at small offset frequency referred to as $S_{\delta\alpha}^{\max}$ in the inset of Fig. 2.

We compare the evolution of the measured response-to-noise parameters to their theoretical evolutions with current I given by Eqs. (7)–(9).

TABLE I. Vortex dynamics parameters with $R = 250$ nm, $T = 300$ K, and $H_\perp = 4.4$ kOe. Experimental values extracted from the fit of the response-to-noise parameters from Eqs. (7)–(9), and theoretical values assuming the analytical expressions in Appendix B.

		Experimental	Theoretical
κ_{ms}	(kg s^{-2})	4.4×10^{-5}	4.1×10^{-5}
κ_{oe}	(kg m^2 A^{-1} s^{-2})	15×10^{-16}	7.2×10^{-16}
G	(kg rad^{-1} s^{-1})	7.4×10^{-14}	5.3×10^{-14}
D	(kg rad^{-1} s^{-1})	19×10^{-16}	8.8×10^{-16}
a_j	(kg m^2 A^{-1} s^{-2})	13×10^{-17}	6.6×10^{-17}
κ'_{ms}	(kg s^{-2})	2.2×10^{-4}	0.1×10^{-4}
κ'_{oe}	(kg m^2 A^{-1} s^{-2})	-1.1×10^{-14}	-3.6×10^{-16}
ξ		2.0	0.6

The experimental data (carrier frequency f_c, normalized amplitude s_0, and response-to-noise parameters f_p, Δf_0, and ν) are fitted with the Eqs. (2), (5), and (7)–(9) as detailed in Appendix C (see solid lines in Fig. 4) with good agreement except for the normalized dimensionless nonlinear frequency shift ν. From the fitting parameters, we derive the quantities describing the vortex gyrotropic dynamics and list them in Table I. They reproduce well the gyrotropic dynamic parameter values calculated from analytical expressions (see Appendix B) except for the nonlinearities of the confinement (κ'_{ms}, κ'_{oe}) and the damping ξ. This discrepancy may arise from the transition to a different dynamic regime in region ② that is not well described by the model, or from a limitation in the theoretical predictions that takes into account nonlinearities only up to the second order.

With regard to the analytical model, we assert the advantages of vortex-based STNO. The first is that the generation linewidth in the linear regime $2\Delta f_0$ is of the order of 100 kHz instead of 1 MHz for uniform-based STNO. Thus, vortex-based STNOs present the lower level of intrinsic phase noise. In addition, although the level of amplitude noise and the normalized dimensionless nonlinear frequency shift are of the same order of magnitude, the conversion factor of amplitude-to-phase noise $\nu f_p = N p_0/\pi$ [see Eq. (11)] is of the order of 10^6 instead of 10^8 for uniform-based STNOs. It follows that the measured linewidth Δf for vortex-based STNOs is at least one order of magnitude smaller than uniform-based STNO linewidth.

Moreover, we propose possible improvements to the vortex-based STNO features. Considering that the vortex-based STNO linewidth Δf is at least one order of magnitude higher than $2\Delta f_0$ at room temperature, the linewidth can be significantly reduced. By suppressing the amplitude-to-phase noise conversion, the phase noise would be equal to $2\Delta f_0$. To reduce the linewidth Δf, one can reduce the intrinsic linewidth Δf_0 or the amplitude-to-phase noise conversion (proportional to the amplitude noise level $S_{\delta\alpha}^{\max}$ and the conversion factor of amplitude-to-phase noise νf_p) through the fabrication techniques increasing the spin polarization efficiency a_j or decreasing the damping D [see Eqs. (7)–(9)]. To change ν, there is a need for a modification of the magnetic disk shape and material, because this term is linked to the nonlinearities specific to the system. Furthermore, it is possible to decrease

the phase noise with an external feedback or excitation: as recently shown in experiments [40], the parametrically excited gyrotropic motion demonstrates linewidths of the order of the intrinsic linewidth $2\Delta f_0$. The origin of this low value may be the suppression of the amplitude-to-phase noise conversion.

V. CONCLUSIONS

We investigate how noise affects the spin-transfer-induced vortex magnetization dynamics in a magnetic tunnel junction. From single-shot time domain measurements, we measure the amplitude noise and phase noise associated with the gyrotropic motion of the vortex core for different values of external magnetic field and dc current. We propose a development of the nonlinear auto-oscillator model for the vortex-based STNO where we define the amplitude and phase noise analytical expressions as functions of the response-to-noise parameters f_p, Δf_0, and ν. We show that the amplitude noise and phase noise are well described within the nonlinear auto-oscillator framework. From the comparison of the experiments to the analytical expressions we extract the response-to-noise parameters. Their values and evolutions with current are correlated to theoretical ones with good agreements apart for the nonlinearities. We deduce that the low linewidth of vortex-based STNOs arises from the small value of the amplitude-to-phase noise conversion factor $\nu f_p = Np_0/\pi$ and generation linewidth in the linear regime $2\Delta f_0$. The major noise contribution to the linewidth broadening is due to the amplitude-phase coupling and has to be suppressed if one wants to reduce significantly the linewidth.

ACKNOWLEDGMENTS

The authors acknowledge A. S. Jenkins, R. Lebrun, M. Quinsat, and A. Slavin for fruitful discussions; Y. Nagamine, H. Maehara, and K. Tsunekawa of CANON ANELVA for preparing the MTJ films; and the financial support from ANR agency (SPINNOVA ANR-11-NANO-0016) and EU FP7 grant (MOSAIC No. ICT-FP7- n.317950). E.G. acknowledges CNES and DGA for financial support.

APPENDIX A: RELATION BETWEEN THE MEASURED VOLTAGE, THE VORTEX CORE POSITION, AND THEIR NOISE

The STNO is an oscillating resistance $R_s(t)$ where

$$R_s(t) = R_0 + \Delta R(t),$$

with R_0 the resistance mean value and $\Delta R(t)$ the oscillating part. Thus, the STNO is equivalent to the resistance R_0 in series with a voltage generator $e(t) = \Delta R(t) I$ (with I the dc current injected in the STNO). The generator voltage that depends on the vortex core position can be expressed as

$$e(t) = \lambda s_0 \left(1 + \frac{\delta s(t)}{s_0}\right) \cos[\dot{\theta} t + \delta\theta(t)],$$

with a magnetoresistive factor λ, in which the influence of the perpendicular magnetic field $H_\perp$ on the magnetization of the layers and of the electrical current I are also taken into account, as

$$\lambda = \frac{I \Delta R_{p-ap}(I)}{2} \beta \sqrt{\left[1 - \left(\frac{H_\perp}{4\pi M_S^{\mathrm{SAF}}}\right)^2\right]\left[1 - \left(\frac{H_\perp}{4\pi M_S^{\mathrm{free}}}\right)^2\right]},$$

with the difference of resistance between the antiparallel state and the parallel state $\Delta R_{p-ap}(I)$ at a given I, the free layer saturation magnetization M_S^{free}, the SAF layer saturation magnetization M_S^{SAF}, and the conversion factor of the vortex core displacement into magnetization change [41] $\beta = \frac{2}{3}$ valid for displacements up to 60% of the dot radius.

The input measurement voltage $V(t)$ is expressed as

$$V(t) = V_0 [1 + \delta\alpha(t)] \cos[2\pi f t + \delta\phi(t)],$$

and the relationship between the measured voltage and the generator bias voltage is

$$V(t) = \frac{R_{\mathrm{load}}}{R_{\mathrm{load}} + R_0} e(t)$$

due to the impedance mismatch, where R_{load} is the resistance input of the measurement device (for our experiments $R_{\mathrm{load}} = 50\Omega$).

Finally we obtain

$$V_0 = \frac{R_{\mathrm{load}}}{R_{\mathrm{load}} + R_0} \lambda s_0, \quad \delta\alpha(t) = \frac{\delta s(t)}{s_0},$$
$$2\pi f = \dot{\theta}, \quad \delta\phi(t) = \delta\theta(t).$$

Thus the voltage normalized amplitude noise is equal to the magnetization normalized amplitude noise and the voltage phase noise is equal to the magnetization phase noise. We express the measured integrated power P_{int} as

$$P_{\mathrm{int}} = \frac{R_{\mathrm{load}}}{(R_{\mathrm{load}} + R_0)^2} \langle V^2 \rangle = \frac{R_{\mathrm{load}}}{2(R_{\mathrm{load}} + R_0)^2} (\lambda s_0)^2. \quad \text{(A1)}$$

APPENDIX B: ANALYTICAL EXPRESSIONS OF THE VORTEX DYNAMICS PARAMETERS

To express the influence of the perpendicular magnetic field $H_\perp$ on the free layer magnetization, we define

$$\theta_0 = \arccos\left(\frac{H_\perp}{4\pi M_S^{\mathrm{free}}}\right),$$

with M_S^{free} the saturation magnetization of the free layer.

The vortex core magnetostatic confinement stiffness and its nonlinear coefficient are:

$$\kappa_{\mathrm{ms}} = \frac{10}{9} \mu_0 M_S^{\mathrm{free}\,2} \frac{L^2}{R} \sin^2\theta_0,$$
$$\kappa'_{\mathrm{ms}} = 0.25 \kappa_{\mathrm{ms}}.$$

TABLE II. Magnetic parameters used for theoretical estimations.

α		0.01
M_S^{SAF}	(A m^{-1})	10.1×10^5
M_S^{free}	(A m^{-1})	6.5×10^5
P_{spin}		0.26
b	(nm)	33

The vortex core confinement stiffness due to Zeeman interaction with the Oersted field and its nonlinear coefficient are:

$$\kappa_{\mathrm{oe}} = 0.85C\mu_0 M_S^{\mathrm{free}} LR\sin\theta_0,$$
$$\kappa'_{\mathrm{oe}} = -0.42C\mu_0 M_S^{\mathrm{free}} LR\sin\theta_0.$$

The gyrovector norm is:

$$G = 2\pi\frac{LM_S^{\mathrm{free}}}{\gamma}(1-\cos\theta_0).$$

The damping coefficient is:

$$D = 2\pi\frac{\alpha\eta LM_S^{\mathrm{free}}}{\gamma},$$
$$\text{with}\quad \eta = \left(\ln(R/2b) - \frac{1}{4}\right)\sin^2\theta_0.$$

The spin-transfer-torque efficiency is:

$$a_j = \pi\frac{\hbar P_{\mathrm{spin}}}{2|e|}p_z\sin^2\theta_0,$$
$$\text{with}\quad p_z = \frac{H_\perp}{4\pi M_S^{\mathrm{SAF}}}.$$

where μ_0 the vacuum permeability, L the thickness of the free layer, R the radius of the free layer, γ the gyromagnetic ratio, α the Gilbert damping, b the vortex core radius $\hbar$ the reduced Planck constant, P_{spin} the spin polarization of the SAF layer, e the electric charge, and M_S^{SAF} the SAF magnetization. All these coefficients are calculated using the magnetic parameters in Table II.

APPENDIX C: METHOD TO FIT THE EXPERIMENTAL RESPONSE-TO-NOISE PARAMETERS

The response-to-noise parameter evolutions are expressed as functions of current I as

$$\pi f_p = -\frac{D\kappa_{\mathrm{ms}}}{G^2} + \left(\frac{a_j}{G\pi R^2} - \frac{D\kappa_{\mathrm{oe}}}{G^2\pi R^2}\right)I, \tag{C1}$$

$$2\Delta f_0 = \frac{k_B T}{\pi R^2}\frac{D}{G^2}\left(\frac{1}{p_0} + \frac{1}{\nu}\frac{G\kappa'_{\mathrm{ms}}}{D\kappa_{\mathrm{ms}}}h(I)\right), \tag{C2}$$

$$\nu = \frac{\zeta}{\frac{D}{G}(\zeta+\xi)} = \frac{G}{D}\frac{1}{1+\xi\frac{\kappa_{\mathrm{ms}}}{\kappa'_{\mathrm{ms}}}h(I)}, \tag{C3}$$

where

$$h(I) = \frac{1+\kappa_{\mathrm{oe}}I/\pi R^2\kappa_{\mathrm{ms}}}{1+\kappa'_{\mathrm{oe}}I/\pi R^2\kappa'_{\mathrm{ms}}}, \tag{C4}$$

and the carrier frequency as

$$f_c = \frac{\kappa_{\mathrm{ms}}}{2\pi G}\left[\left(1+\frac{\kappa_{\mathrm{oe}}I}{\kappa_{\mathrm{ms}}\pi R^2}\right) + \frac{\kappa'_{\mathrm{ms}}}{\kappa_{\mathrm{ms}}}p_0\left(1+\frac{\kappa'_{\mathrm{oe}}I}{\kappa'_{\mathrm{ms}}\pi R^2}\right)\right]. \tag{C5}$$

The experimental data are fitted with the previous equations to extract the gyrotropic motion quantities as the following:

(i) We fit f_p evolution with Eq. (C1) from which we extract $\frac{D\kappa_{\mathrm{ms}}}{G^2}$ and $\frac{a_j}{G\pi R^2} - \frac{D\kappa_{\mathrm{oe}}}{G^2\pi R^2}$.

(ii) We fit the linear part of the frequency $f_c - \frac{\nu f_p}{2}$ from which we extract $\frac{\kappa_{\mathrm{ms}}}{2\pi G}$ and $\frac{\kappa_{\mathrm{oe}}}{\pi R^2\kappa_{\mathrm{ms}}}$.

(iii) We fit the frequency carrier with Eq. (C5) assuming the values of the parameters extracted above and injecting the oscillation power p_0. We deduce $\frac{\kappa'_{\mathrm{ms}}}{\kappa_{\mathrm{ms}}}$ and $\frac{\kappa'_{\mathrm{oe}}}{\pi R^2\kappa'_{\mathrm{ms}}}$.

(iv) We fit the evolution of ν with Eq. (C3) when injecting the parameters above, from which we deduce $\frac{G}{D}$.

(v) We fit the evolution of Δf_0 with Eq. (C2) knowing the parameters extracted above and injecting ν and the oscillation power p_0. From this we extract $\frac{k_B T}{\pi R^2}\frac{D}{G^2}$.

The oscillation power $p_0 = {s_0}^2$ is evaluated with s_0 calculated as presented in Appendix A.

[1] L. Berger, Phys. Rev. B **54**, 9353 (1996).
[2] J. C. Slonczewski, J. Magn. Magn. Mater. **159**, L1 (1996).
[3] A. A. Tulapurkar, Y. Suzuki, A. Fukushima, H. Kubota, H. Maehara, K. Tsunekawa, D. D. Djayaprawira, N. Watanabe, and S. Yuasa, Nature **438**, 339 (2005).
[4] J. Katine and E. E. Fullerton, J. Magn. Magn. Mater. **320**, 1217 (2008).
[5] S. I. Kiselev, J. C. Sankey, I. N. Krivorotov, N. C. Emley, R. J. Schoelkopf, R. A. Buhrman, and D. C. Ralph, Nature **425**, 380 (2003).
[6] W. H. Rippard, M. R. Pufall, S. Kaka, S. E. Russek, and T. J. Silva, Phys. Rev. Lett. **92**, 027201 (2004).
[7] Q. Mistral, M. van Kampen, G. Hrkac, J.-V. Kim, T. Devolder, P. Crozat, C. Chappert, L. Lagae, and T. Schrefl, Phys. Rev. Lett. **100**, 257201 (2008).
[8] A. Dussaux, B. Georges, J. Grollier, V. Cros, A. Khvalkovskiy, A. Fukushima, M. Konoto, H. Kubota, K. Yakushiji, S. Yuasa, K. Zvezdin, K. Ando, and A. Fert, Nat. Commun. **1**, 8 (2010).
[9] Q. Mistral, J.-V. Kim, T. Devolder, P. Crozat, C. Chappert, J. A. Katine, M. J. Carey, and K. Ito, Appl. Phys. Lett. **88**, 192507 (2006).
[10] K. Kudo, T. Nagasawa, R. Sato, and K. Mizushima, J. Appl. Phys. **105**, 07D105 (2009).
[11] B. Georges, J. Grollier, V. Cros, A. Fert, A. Fukushima, H. Kubota, K. Yakushijin, S. Yuasa, and K. Ando, Phys. Rev. B **80**, 060404 (2009).
[12] R. P. Cowburn, D. K. Koltsov, A. O. Adeyeye, M. E. Welland, and D. M. Tricker, Phys. Rev. Lett. **83**, 1042 (1999).
[13] T. Shinjo, T. Okuno, R. Hassdorf, K. Shigeto, and T. Ono, Science **289**, 930 (2000).
[14] A. A. Thiele, Phys. Rev. Lett. **30**, 230 (1973).

[15] J. C. Sankey, I. N. Krivorotov, S. I. Kiselev, P. M. Braganca, N. C. Emley, R. A. Buhrman, and D. C. Ralph, Phys. Rev. B **72**, 224427 (2005).
[16] P. Bortolotti, A. Dussaux, J. Grollier, V. Cros, A. Fukushima, H. Kubota, K. Yakushiji, S. Yuasa, K. Ando, and A. Fert, Appl. Phys. Lett. **100**, 042408 (2012).
[17] B. Picinbono, IEEE Trans. Sign. Proc. **45**, 552 (1997).
[18] L. Bianchini, S. Cornelissen, J.-V. Kim, T. Devolder, W. van Roy, L. Lagae, and C. Chappert, Appl. Phys. Lett. **97**, 032502 (2010).
[19] M. Quinsat, D. Gusakova, J. F. Sierra, J. P. Michel, D. Houssameddine, B. Delaet, M.-C. Cyrille, U. Ebels, B. Dieny, L. D. Buda-Prejbeanu, J. A. Katine, D. Mauri, A. Zeltser, M. Prigent, J.-C. Nallatamby, and R. Sommet, Appl. Phys. Lett. **97**, 182507 (2010).
[20] K. Mizushima, K. Kudo, and R. Sato, J. Magn. Magn. Mater. **316**, e960 (2007).
[21] V. Tiberkevich, A. Slavin, and J.-V. Kim, Appl. Phys. Lett. **91**, 192506 (2007).
[22] J.-V. Kim, V. Tiberkevich, and A. N. Slavin, Phys. Rev. Lett. **100**, 017207 (2008).
[23] A. Slavin and V. Tiberkevich, IEEE Trans. Magn. **45**, 1875 (2009).
[24] T. J. Silva and M. W. Keller, IEEE Trans. Magn. **46**, 3555 (2010).
[25] A. V. Khvalkovskiy, J. Grollier, A. Dussaux, K. A. Zvezdin, and V. Cros, Phys. Rev. B **80**, 140401 (2009).
[26] P. K. Muduli, O. G. Heinonen, and J. Åkerman, Phys. Rev. Lett. **108**, 207203 (2012).
[27] A. Dussaux, A. V. Khvalkovskiy, P. Bortolotti, J. Grollier, V. Cros, and A. Fert, Phys. Rev. B **86**, 014402 (2012).
[28] M. L. Schneider, W. H. Rippard, M. R. Pufall, T. Cecil, T. J. Silva, and S. E. Russek, Phys. Rev. B **80**, 144412 (2009).
[29] J. F. Sierra, M. Quinsat, F. Garcia-Sanchez, U. Ebels, I. Joumard, A. S. Jenkins, B. Dieny, M.-C. Cyrille, A. Zeltser, and J. A. Katine, Appl. Phys. Lett. **101**, 062407 (2012).
[30] M. W. Keller, M. R. Pufall, W. H. Rippard, and T. J. Silva, Phys. Rev. B **82**, 054416 (2010).
[31] M. W. Keller, A. B. Kos, T. J. Silva, W. H. Rippard, and M. R. Pufall, Appl. Phys. Lett. **94**, 193105 (2009).
[32] J.-V. Kim, Phys. Rev. B **73**, 174412 (2006).
[33] J.-V. Kim, Q. Mistral, C. Chappert, V. S. Tiberkevich, and A. N. Slavin, Phys. Rev. Lett. **100**, 167201 (2008).
[34] V. S. Tiberkevich, A. N. Slavin, and J.-V. Kim, Phys. Rev. B **78**, 092401 (2008).
[35] M. Quinsat, V. Tiberkevich, D. Gusakova, A. Slavin, J. F. Sierra, U. Ebels, L. D. Buda-Prejbeanu, B. Dieny, M.-C. Cyrille, A. Zelster, and J. A. Katine, Phys. Rev. B **86**, 104418 (2012).
[36] A. Dussaux (unpublished).
[37] Y.-S. Choi, S.-K. Kim, K.-S. Lee, and Y.-S. Yu, Appl. Phys. Lett. **93**, 182508 (2008).
[38] A. Hamadeh, G. De Loubens, O. Klein, V. V. Naletov, R. Lebrun, N. Locatelli, J. Grollier, and V. Cros, arXiv:1310.4913.
[39] T. Arakawa, T. Tanaka, K. Chida, S. Matsuo, Y. Nishihara, D. Chiba, K. Kobayashi, T. Ono, A. Fukushima, and S. Yuasa, Phys. Rev. B **86**, 224423 (2012).
[40] P. Bortolotti, E. Grimaldi, A. Dussaux, J. Grollier, V. Cros, C. Serpico, K. Yakushiji, A. Fukushima, H. Kubota, R. Matsumoto, and S. Yuasa, Phys. Rev. B **88**, 174417 (2013).
[41] K. Y. Guslienko, B. A. Ivanov, V. Novosad, Y. Otani, H. Shima, and K. Fukamichi, J. Appl. Phys. **91**, 8037 (2002).